

WPT SAR Compliance Simulation Report for PGT-N19

Model Name:
PGT-N19

FCC ID:
2AYGCPGT-N19

Date of Simulation:
2023/01/10-2023/1/20

Location:
Honor Device Co., Ltd., Shenzhen, China

Contents

1. Introduction	2
2. Product Information	3
3. Simulation Tool and Model.....	6
3.1 Simulation Tool	6
3.2 Mesh and Convergence Criteria	6
3.3 Power Density Calculation	7
3.4 3D Model	8
4. SAR Simulation Step	9
4.1 SAR Simulations Methodology.....	9
4.1.1 Boundary Conditions.....	10
4.1.2 Source Excitation Condition.....	10
4.1.3 Simulation Completion Conditions.....	10
4.2 H-field Strength Measurement and Simulations	10
4.3 SAR simulation	14
4.4 Calculation	18
Annex A: Specific information for SAR computational modelling.....	19
A.1 Code performance validation.....	19
A.1.1 Propagation in a rectangular waveguide.....	19
A.1.2 Planar dielectric boundaries	24
A.2 Generic dipole	28
A.3 Total Computational Uncertainty	30

1.Introduction

This report demonstrates RF exposure compliance using SAR simulation for WPT of PGT-N19 (FCC ID: 2AYGCPGT-N19)

The device is a mobile phone supporting wireless charging function. In addition to being charged by the WPT charger, one Phone can also be used as a WPT charger to wirelessly charge another Phone. According to §2.1093 (certification for portable devices below 4 MHz), the Phone operating at 110-145 kHz should demonstrate RF exposure compliance to the 1.6 W/kg localized 1-g SAR limit. Therefore, to be conservative, we consider the phone to be a portable device as a wireless charger. For portable devices, an accurate SAR value for the WPT transmitter is required. Since SAR test tools is not suitable for use below 100 MHz, we apply SAR numerical modeling to obtain SAR values.

The following sections describe the modeling, measured H-field, simulated H-field, and simulated SAR.

2.Product Information

The device is a mobile phone. There are two types of wireless charging usage scenarios:

a) Used as a client device (Rx mode)

When the mobile phone needs to be recharged, it is used as a client device (Rx). The DUT should be placed directly in contact with the charging area of TX device (such as wireless charging pad)

b) Used as a transmitter device (Tx mode)

The DUT can also provide wireless charging for another mobile phone. The DUT is used as a wireless charging transmitter device (Tx) in this usage scenario.

The wireless coil used by the mobile phone as the client device (Rx) and the transmitting device (Tx) is the same. details of the wireless charging coil are shown in Table 1. The device has only one coil and the number of turns for the primary coil is 10 turns and measures 9.46 μH in the air. The primary coil has 1.4 A current. The coil module is composed of an FPC coil.

Coil Winding Type	FPC double-layer copper-plated traces
Inner Radius	11 mm
Outer Radius	24 mm
Cross Section	Rectangular
Thickness	0.149

Table 1. Details of the wireless charging coil

Table 2 is some important parameters when using wireless charging and the maximum excursion in wireless charging mode. These can help us find the worst-case RF exposure scenarios. The operating frequency of the device is

between 110 kHz and 148 kHz. When wireless charging, regardless of other factors, the horizontal offset can reach 8 mm

Item	Description
Tx Power	2.5, 5 and 7.5 Watt
Operating Frequency	110 kHz-145 kHz
Communication Method	FSK-> Charger to Phone ASK-> Phone to Phone
Horizontal Offset	X,Y 8 mm

Table 2. Some parameters when using wireless charging

The transfer system includes only single primary coil. The device only support one-to-one pairing with the client device. The wireless charging coil is located at the back side of the DUT (as the figure below). The coil module is composed of an FPC coil and a Nanocrystalline magnetic shielding material, and the magnetic shielding material blocks the magnetic field in the direction of the battery, and the radiation direction of the wireless charging is towards the back cover of the phone.

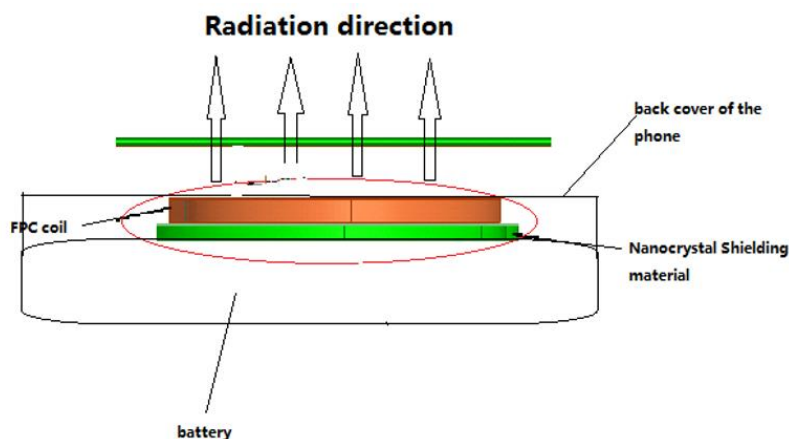


Figure 1 Coil Schematic

Tx and Rx communicate using a single channel, and all Rx-Tx and Tx-Rx communication physical channels are wireless signals transmitted by Tx. When

the Phone is used as a Tx, it is necessary to manually open the wireless charging software switch. The DUT inside will change the circuit to switch to the Tx mode. Then place the client device directly in contact with the back side charging area of the DUT. The Tx will send PING to detect the client device (RX). Once Rx is powered by Tx in the charging area, Tx-Rx device will enter power transfer phase. As shown in Table 2, the output power of Tx has three gears of 2.5, 5 and 7.5 W, but the maximum output power of 7.5 W can only be achieved when the power of Tx is greater than 90% and the adapter (Max output) is connected.

3. Simulation Tool and Model

3.1 Simulation Tool

For the calculation of the magnetic field value and SAR simulation method of the mobile phone with the function of wireless reverse charging, this article uses the electromagnetic module in COMSOL Multiphysics 6.0. COMSOL Multiphysics 6.0 is one of several commercial tools for 3D electromagnetic simulation of wireless charging. The frequency domain solvers in COMSOL Multiphysics 6.0 are based on finite element (FEM) solutions.

3.2 Mesh and Convergence Criteria

To use FEM to calculate the magnetic field value and SAR value of wireless charging and reverse charging, it is necessary to divide the mobile phone, human tissue, and surrounding environment into multiple small units. The physical quantities on the nodes and edges of each small unit can be used as the calculated magnetic field value and the process of dividing the unknown SAR value into small cells is called meshing. To calculate the objective of the solution, the COMSOL Multiphysics 6.0 adaptive meshing technique was used. COMSOL Multiphysics 6.0 generates an initial mesh based on the minimum value of the wavelength of the electromagnetic field and the size of the target body, calculates the energy error during each iteration, and performs adaptive refinement and refinement for the regions with large errors. The determination of the number of calculation iterations in COMSOL Multiphysics 6.0 and the completion of the final iterative calculation process are called the convergence process. The convergence criterion tolerance is used to judge whether the convergence process is over. During the calculation process, the iterative adaptive grid process is performed until the convergence criterion tolerance is met. In COMSOL Multiphysics 6.0, the accuracy of the convergence results depends on the tolerance. Figure 2 is an example of computing an object

adaptive mesh.

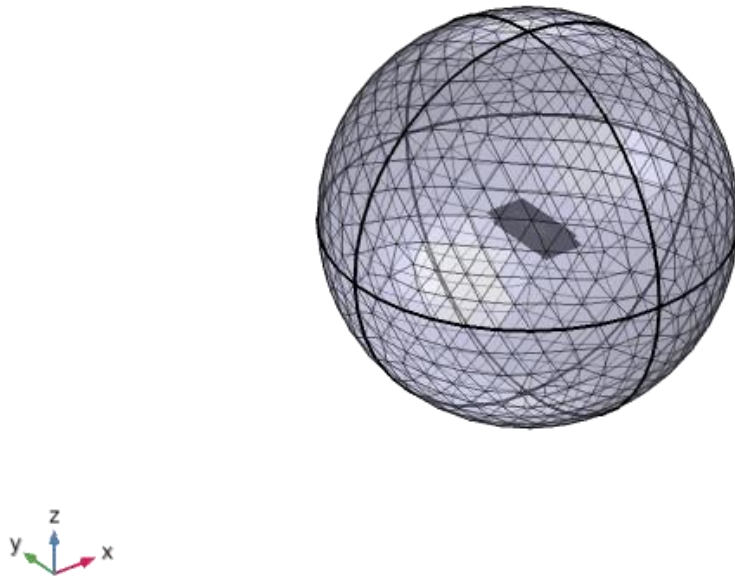


Figure 2. an example of computing an object adaptive mesh.

3.3 Power Density Calculation

By solving the three-dimensional wireless charging reverse charging simulation model, the numerical values of the electric field and magnetic field physical quantities at each position in the space can be obtained. In order to calculate the power density, two physical quantities need to be extracted: the electric field (E) and the magnetic field (H). The actual power density dissipated as the complex conjugate product of the electric field E and the magnetic field H yields the real part of the vector (S) as follows:

$$\langle \vec{S} \rangle = \text{Re} \left(\frac{1}{2} \vec{E} \times \vec{H}^* \right)$$

$\langle \vec{S} \rangle$ is the peak point power density at the node is calculated for each mesh, which can be obtained directly from COMSOL Multiphysics 6.0.

From the point power density $\langle \vec{S} \rangle$, the calculation formula of the average power density of the space volume V is as follows:

$$P_{Loss} = \frac{1}{V} \iiint_0^V \langle \vec{S} \rangle \cdot dV$$

Here, the spatial average power density P_{Loss} is the total power density value of the x, y, and z components of the point power density, and the estimated volume is 1 cm^3 .

3.4 3D Model

Figure 3 shows the 3D simulation model of two mobile phones for wireless reverse charging. The simulation model includes most of the finishing structure of the device: PCB, metal frame, battery, metal structure, wireless charging coil of mobile phone and magnetic conductive material, etc. Due to the existence of the metal structure of the camera module, the backs of the two mobile phones cannot be completely overlapped. The wireless coil is on the back of the phone.

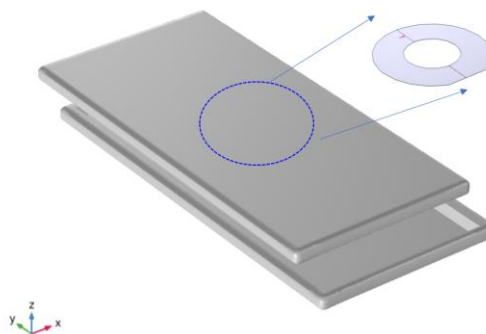


Figure 3. The 3D simulation model

4. SAR Simulation Step

4.1 SAR Simulations Methodology

The following Figure are taken to show the validity of the model used for SAR simulations:

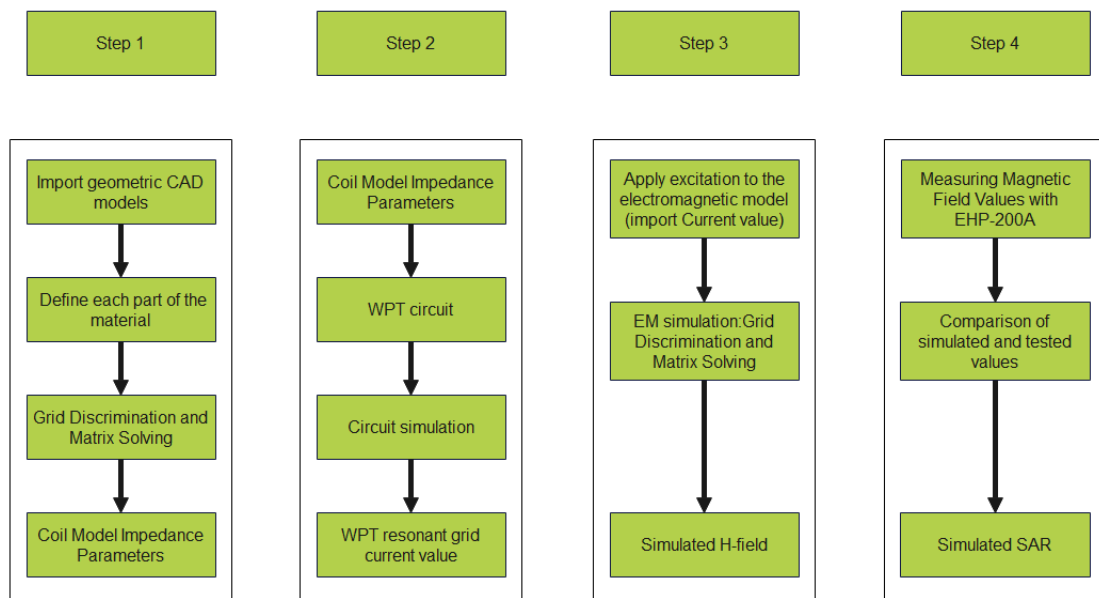


Figure 4. The steps of SAR simulation

First, import the CAD model of the mobile phone into the software for material definition and mesh division to calculate the impedance of the coil. Then import the coil impedance into the WPT circuit to calculate the current value of the WPT circuit. And then, the electromagnetic model is excited by the current, and the simulated value of the field strength can be obtained. The accuracy of the wild goose array simulation is compared by the simulation and the actual test, and finally the SAR value is simulated.

4.1.1 Boundary Conditions

FEM-based electromagnetic simulation tools need to impose boundary conditions on the simulation model, and the boundary conditions imposed are the first type of boundary conditions (Dirichlet boundary conditions). COMSOL Multiphysics 6.0 supports the direct application of Dirichlet boundary conditions. To ensure the accuracy of the results, the Dirichlet boundary is a sphere with a radius of 40 cm, which is sufficient to attenuate the energy of the magnetic field and electric field to ensure the accuracy of the results.

4.1.2 Source Excitation Condition

The excitation conditions for wireless reverse charging calculation are obtained by the circuit as shown in Figure 7. Calculated current excitation results of the circuit can be applied directly at the coil port. After completing a 3D full-wave electromagnetic simulation of the modeled structure, the current to the coil can be loaded using the COMSOL Multiphysics 6.0 "coil excitation" function. Since COMSOL Multiphysics 6.0 uses a FEM solver based on the frequency domain analysis method, the input source of the coil excitation is calculated using a sinusoidal waveform for the operating frequency.

4.1.3 Simulation Completion Conditions

The simulation completion condition in COMSOL Multiphysics 6.0 is defined as a tolerance smaller than the desired value. The simulation result for this report is to set the tolerance to 0.001.

4.2 H-field Strength Measurement and Simulations

We use the Narda EHP-200A to measure the actual H-field strength of the DUT. EHP-200A E-H fields analyzer has been designed for accurate

measurements of both electric (0.02 to 1000 V/m) and magnetic (3 mA/m to 300 A/m) fields in the frequency range 9 kHz to 30 MHz. Both the field sensors and the electronic measuring circuitry are accommodated in a robust housing. Measurements are given total value (peak and average), with exceptional flatness and linearity. The probe specifications of H-field mode are giving below:

Test Mode	Magnetic Field Mode A
Frequency range	9 kHz-3 MHz
Measurement range @10 kHz RBW	30 mA/m – 300 A/m
Dynamic range	> 80 dB
Resolution	1 mA/m
Sensitive @10 kHz RBW	30 mA/m
Flatness	0.8 dB
Span	0 to Full Span

Table 3 The information of EHP-200A for H-field measurement

For the EHP-200A the sensitive element is located approximately 8 mm bellow the external surface like Figure 5, therefore, when comparing the simulated values, the simulated field strength should be obtained at 8 mm from the surface of the DUT. Per TCB Workshop April 2022, If the center of the probe sensing element is more than 5 mm from the probe outer edge, the field strengths need to be estimated for the positions that are not reachable (from the surface, in 2 cm increments)

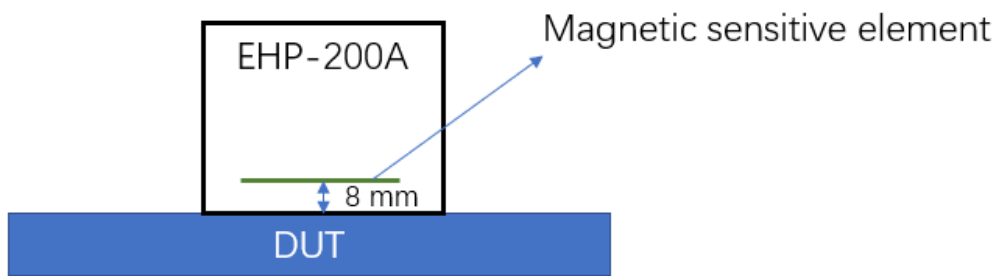


Figure 5. The located of sensitive element

The scene where one mobile phone charges the other mobile phone occurs when the backs of the two mobile phones are close to each other, and due to the camera module, the camera cannot appear on the same side, like Figure 9 shown. The test position is as shown in the figure, which is given according to Tx DUT.

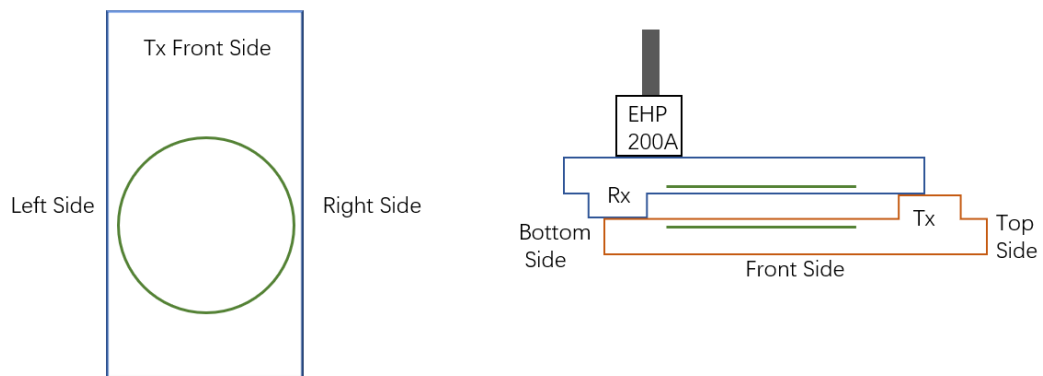


Figure 6. DUT test diagram

To accurately measure the value of the magnetic field strength, we set the measurement step to 2 mm, and the test surface is the Front, Right and Left sides that conform to the Portable device.

The H-field simulations are conducted using commercially available software COMSOL. To validate the simulation model, H-field measurements are made on the DUT (as Figure 6 shown) and compared to the simulated results. The validated model is then used for SAR simulations.

Test/simulation Side	Test Channel/Freq (KHz)	Text Tx Power(W)	Test Result(A/m)	Simulation Result(A/m)	Gap
Front Side	112.8	5	2.24	2.79	24.5%
Left Side	112.8	5	2.55	3.16	24.0%
Right Side	112.8	5	3.21	3.74	16.5%
Front Side	112.8	7.5	2.97	3.60	21.2%
Left Side	112.8	7.5	3.71	4.12	11.0%
Right Side	112.8	7.5	3.94	4.83	22.5%

Table 4. The test result and simulation result of H-field

The result is shown above. It can be seen that the biggest gap between simulation and test at 5w is only 24.5%, which is far below the requirement of 30% (per April 27, 2022, TCB Workshop). And the worst case occurs at 7.5W. The H-field strength values of the four sides are in good agreement with the simulated values. So, this mode can be used to calculate SAR values.

Per TCB Workshop April 2022, If the center of the probe sensing element is more than 5 mm from the probe outer edge, the field strengths need to be estimated for the positions that are not reachable (from the surface, in 2 cm increments). Therefore, we did a simulation test comparison from 8mm (the distance between the magnetic induction unit from the DUT surface) to 18 cm on the Frontside surface of 5W and 7.5W. The results are shown in the following figures The graph show good correlation between the measurements and simulations.

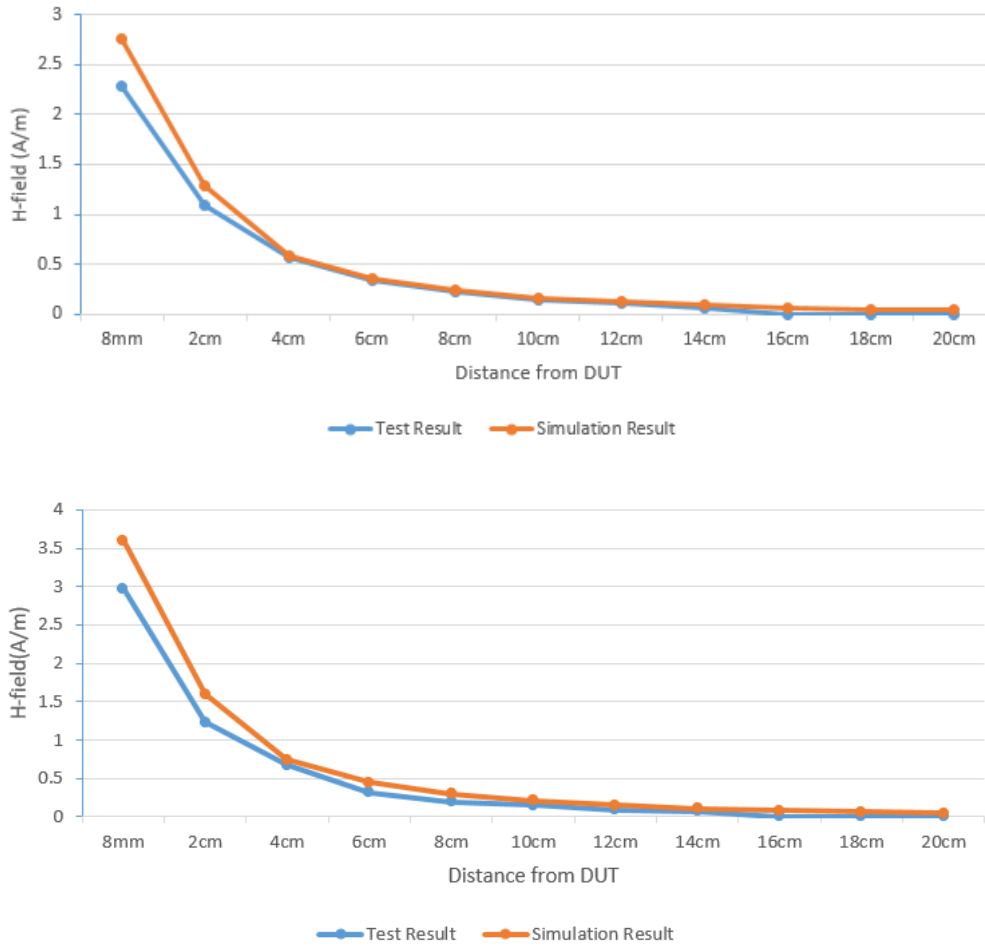


Figure 7. Comparison of test and simulation at different distances at 5W(top), 7.5W(below)

4.3 SAR simulation

The SAR simulations are conducted using commercially available software COMSOL by same model. For this simulation, a phantom is added in contact with the DUT.

The following steps are used for accurate SAR simulation:

- 1) Homogenous tissue material is used as liquid for desired frequency.
- 2) Power loss in phantom is calculated.

3) SAR can be calculated by the Equation:

$$SAR = \frac{P}{\rho}$$

where P is the Power loss density,
and ρ is the tissue density.

4) SAR is averaged over 1 g at 0 mm (FCC).

The portable scene during charging appears when holding a mobile phone to make a call or placing it on the body to use the mobile phone. Therefore, it is necessary to determine the electrical properties of phantom. As mentioned earlier, the frequency of wireless charging is 112.8 kHz, so the electrical characteristics of the body and hand at this frequency are summarized as follows:

Tissue	Thickness (mm)	Permittivity	Conductivity(S/m)
Skin	3	1117	0.001
Muscle	9	7797	0.365
Bone	20	454	0.084
Worst case (Muscle)	/	7797	0.365

Table 5. The electrical characteristics for body layers at 112.8 kHz

Frequency	Tissue	Permittivity	Conductivity(S/m)
110 kHz	Muscle	7786	0.364
112.8 kHz	Muscle	7797	0.365
129 kHz	Muscle	7475	0.368
148 kHz	Muscle	7142	0.372

Table 6. The electrical characteristics for body layers

For hand phantom, compared with body layers, the thickness of each layer is different, but the electrical characteristics are the same at the same frequency, so the same worst case can be used. For all exposure cases, conductivity and permittivity used for the phantoms are fixed as the worst

case (0.365 S/m and 7797), and the phantom size is 360*200*100 mm. Because the operating frequency of the wireless coil is 110-148 kHz, other than 112.8 kHz, the electrochemical properties of 110, 129, and 148 kHz are also listed (Table 6). And the SAR results are peak spatial 1-gram average SAR.

The maximum transmission power of Tx is 7.5W, so the worst case also occurs at 7.5W. First, we did a SAR simulation of 7.5W without horizontal offset working at different frequencies to judge the worst working frequency. The results are shown below:

Simulation Side	Tx Power (W)	Peak Spatial Average SAR over 1-g (W/kg)	Peak Spatial Average SAR over 10-g (W/kg)	Simulated E-field (V/m)	Frequency (kHz)
Fronnd Side	7.5	0.006	0.004	0.65	110
Left Side	7.5	0.014	0.008	0.59	110
Right Side	7.5	0.020	0.012	0.69	110
Top Side	7.5	0.002	0.001	0.17	110
Bottom Side	7.5	0.003	0.001	0.21	110
Fronnd Side	7.5	0.006	0.004	0.64	112.8
Left Side	7.5	0.013	0.008	0.59	112.8
Right Side	7.5	0.020	0.012	0.69	112.8
Top Side	7.5	0.002	0.001	0.16	112.8
Bottom Side	7.5	0.003	0.001	0.21	112.8
Fronnd Side	7.5	0.006	0.004	0.64	129
Left Side	7.5	0.013	0.007	0.58	129
Right Side	7.5	0.019	0.012	0.62	129
Top Side	7.5	0.002	< 0.001	0.15	129
Bottom Side	7.5	0.002	< 0.001	0.17	129
Fronnd Side	7.5	0.005	0.004	0.64	148
Left Side	7.5	0.012	0.007	0.58	148
Right Side	7.5	0.019	0.011	0.62	148
Top Side	7.5	0.002	< 0.001	0.13	148
Bottom Side	7.5	0.002	< 0.001	0.15	148

Table 7 Simulated SAR values at different frequencies without horizontal offset

It can be seen from Table 7 that the worst working condition is at 110kHz. As mentioned earlier, the maximum horizontal offset of the coil is 8mm, so considering the simulated SAR value under different offset situations, the results are as follows:

Simulation Side	Tx Power (W)	Peak Spatial Average SAR over 1-g (W/kg)	Peak Spatial Average SAR over 10-g (W/kg)	Simulated E-field (V/m)	Horizontal (mm)
Fronnd Side	7.5	0.006	0.004	0.65	0
Left Side	7.5	0.014	0.008	0.59	0
Right Side	7.5	0.020	0.012	0.69	0
Top Side	7.5	0.002	0.001	0.17	0
Bottom Side	7.5	0.003	0.001	0.21	0
Fronnd Side	7.5	0.002	0.001	0.63	y-4
Left Side	7.5	0.007	0.005	1.59	y-4
Right Side	7.5	0.008	0.006	1.82	y-4
Top Side	7.5	0.002	0.001	0.25	y-4
Bottom Side	7.5	0.004	0.002	0.37	y-4
Fronnd Side	7.5	0.002	0.002	0.73	y-8
Left Side	7.5	0.009	0.006	1.84	y-8
Right Side	7.5	0.011	0.008	2.13	y-8
Top Side	7.5	0.002	0.001	0.21	y-8
Bottom Side	7.5	0.004	0.002	0.36	y-8
Fronnd Side	7.5	0.012	0.009	2.84	x-4
Left Side	7.5	0.021	0.013	2.21	x-4
Right Side	7.5	0.037	0.016	2.81	x-4
Top Side	7.5	0.003	0.001	0.28	x-4
Bottom Side	7.5	0.005	0.003	0.43	x-4
Fronnd Side	7.5	0.018	0.013	3.1	x-8
Left Side	7.5	0.030	0.020	2.69	x-8
Right Side	7.5	0.056	0.024	3.42	x-8
Top Side	7.5	0.004	0.002	0.33	x-8
Bottom Side	7.5	0.006	0.003	0.57	x-8

Table8 SAR values at different horizontal offsets at 110kHz

From Table 8 we conclude that the maximum SAR occurs when the offset of x is 8mm. SAR plot is show below (Right side with x-8mm offset). The peak spatial 1-g SAR is 0.056 W/kg.

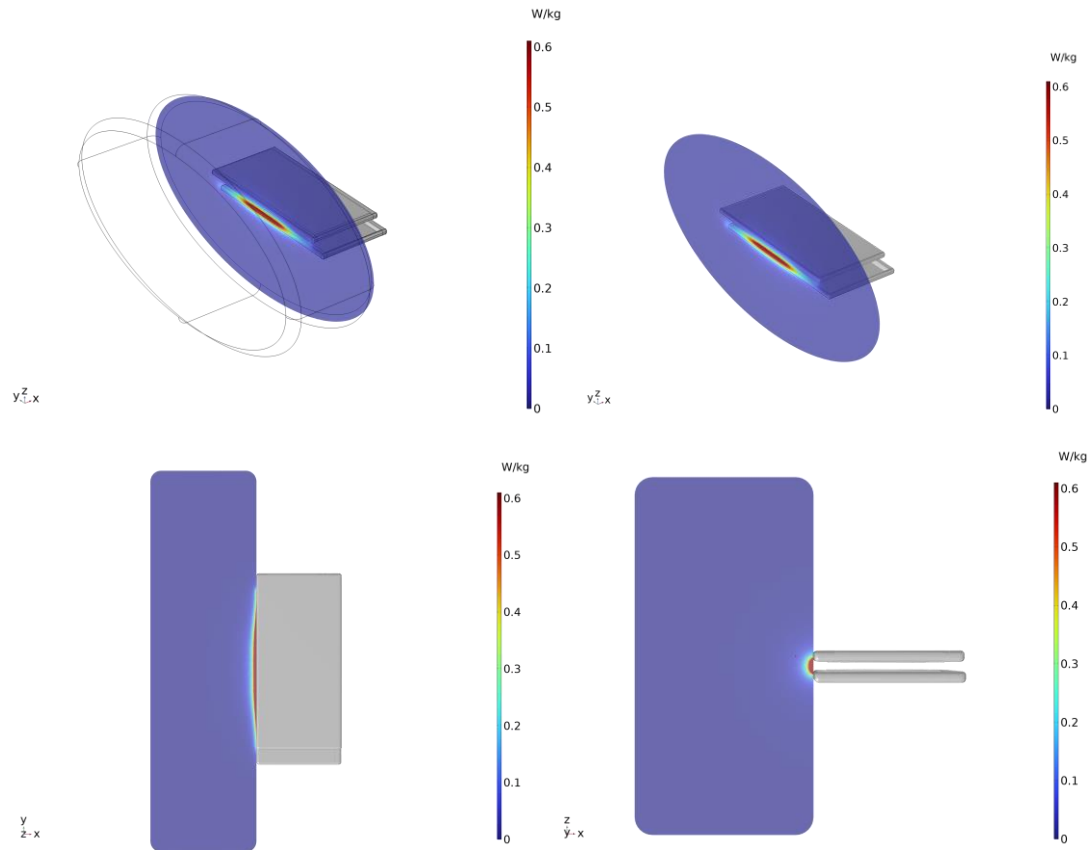


Figure 8 SAR plot bottom view and sectional view with 8 mm offset of x at 110 kHz

4.4 Calculation

The accuracy of the SAR simulations is demonstrated by correlating H-field measurements to simulations in Figure 7, and Table 4. For the nominal case where the phones have a Horizontal offset of x (8 mm) at 110 kHz, the highest peak spatial 1-g average SAR is 0.056W/kg, well below FCC SAR limit 1.6 W/kg.

Annex A: Specific information for SAR computational modelling

A.1 Code performance validation

A.1.1 Propagation in a rectangular waveguide

Need to verify accuracy and convergence for free space and dielectric interfaces. Rectangular waveguides are characterized in terms of wave number and reflection coefficient for the different configurations. Convergence to the physically correct value within a specified tolerance shall be demonstrated for an increasing number (at least three) of DoF.

a) Specification of the waveguide – The rectangular waveguide model is specified with perfectly conducting walls (Figure 9). Its widths in the x- and y-directions are 120 mm and 60 mm, respectively. All directions and dimensions correspond to the coordinate system as shown in Figure 8. The excitation is placed perpendicular to the orientation of the waveguide. The distance from the source to the fields to be recorded shall be 60 mm. The length of the waveguide should be chosen such that reactive fields that can be caused by the truncation of the computational domain do not reach the region where the fields are recorded.

b) TE (transverse electric) polarization – For the TE₁₀ mode, the waveguide shall be terminated with perfect electrical conductors (PEC) as boundary conditions in the x- and ydirections. The E_y components at the source location (Figure 10) shall be excited with the analytical solution of the TE₁₀ mode. This mode can be excited by setting the E_y components at the location of the source or the waveguide port (Figure 10) to the values calculated from Equation (1).

$$E_y = E_0 \sin \frac{x\pi}{w} \quad (1)$$

where E_0 is an arbitrary electric field strength amplitude; x is the location of the E_y component; w is the width of the waveguide.

Alternative methods for the field excitation may be used, such as particular solvers to determine the propagating modes in the waveguide, or preconfigured sources if the code provides them. In any case, it shall be asserted that only the fundamental propagating mode exists at the location where the fields are recorded (Figure 10).

c) TM (transverse magnetic) polarization – For the fundamental TM mode, the waveguide shall be terminated with perfect electrical conductors as boundaries in the x -direction and with perfect magnetic conductors in the y -direction. The fundamental mode for a waveguide consisting of perfect electric-conductor and perfect magnetic-conductor boundaries is the TM₁₀ mode. The mode can be excited by setting the E_x components at the source location (Figure 10) to the values calculated from Equation (2).

$$E_x = E_0 \cos \frac{x\pi}{w} \quad (2)$$

where E_0 is an arbitrary electric field strength amplitude; x is the location of the E_x -component; w is the width of the waveguide.

Alternative methods for the field excitation may be used, such as particular solvers to determine the propagating modes in the waveguide, or preconfigured sources if the code provides them. In any case, it shall be asserted that only the fundamental propagating mode exists at the location where the fields are recorded (Figure 10).

d) Excitation – The TE₁₀ and TM₁₀ modes shall be used as excitations for the waveguide model. The frequencies to be evaluated range from 500 MHz to 2 GHz, with a step size of 25 MHz. Separate simulations shall be carried out for each frequency (61 simulations in total). The frequency range covers both the reactive and the propagating range of the TE₁₀ and TM₁₀ modes in the waveguide.

e) Dielectric parameters – The waveguide shall be simulated with three homogeneous isotropic media (see Figure 9):

$\epsilon_r = 1.0$; $\sigma = 0.0$ S/m;

$\epsilon_r = 2.0$; $\sigma = 0.0$ S/m;

$\epsilon_r = 2.0$; $\sigma = 0.2$ S/m.

f) Field components to be recorded – The Ex components shall be recorded at the locations specified in Figure 10 for the calculation of the dispersion relation as described in the next step

g) Calculation of the dispersion relation – The numerical wave numbers $k_{x,num}$ and $k_{z,num}$ shall be calculated from the Ex components recorded at the locations in Figure 2 using the identities of Equation (3) and Equation (4).

$$k_{x,num} = -\frac{j}{\Delta s} \ln \left(\frac{E_{01} + E_{21} - \sqrt{-4E_{11}^2 + (E_{01} + E_{21})^2}}{2E_{11}} \right) \quad (3)$$

$$k_{z,num} = -\frac{j}{\Delta s} \ln \left(\frac{E_{10} + E_{12} - \sqrt{-4E_{11}^2 + (E_{10} + E_{12})^2}}{2E_{11}} \right) \quad (4)$$

where Δs is the distance between the locations of the recorded components

(30 mm). The numerical wave number can be calculated using Equation (5).

$$k^2 = k_x^2 + k_z^2 \quad (5)$$

The reference solutions of the numerical wave vector for comparison with Equation (4) can be obtained by solving the physically correct dispersion relation of the waveguide, in accordance with Equation (6), Equation (7), and Equation (8).

$$k = \sqrt{\omega\mu_0 (\omega\epsilon_r\epsilon_0 + j\sigma)} \quad (6)$$

$$k_x = \frac{\pi}{w} \quad (7)$$

$$k_z = \sqrt{k^2 - k_x^2} \quad (8)$$

h) Data reporting – The numerical wave numbers for each frequency shall be evaluated as a function of the number of DoF for each frequency. For each waveguide model configuration in Table 10, the maximum deviation from the physical wave number shall be evaluated as a function of frequency. These deviations shall be less than or equal to the tolerances given in Table 9. In addition, the number of DoF at which the tolerance is reached shall be reported for each simulation. The results in Table 9 are acceptable result criteria along with simulation results.

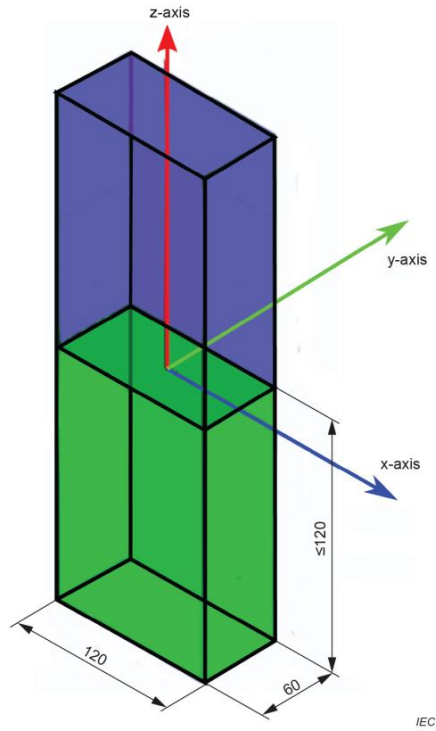


Figure 9 Waveguide filled half with free-space (green) and half with dielectric (blue)

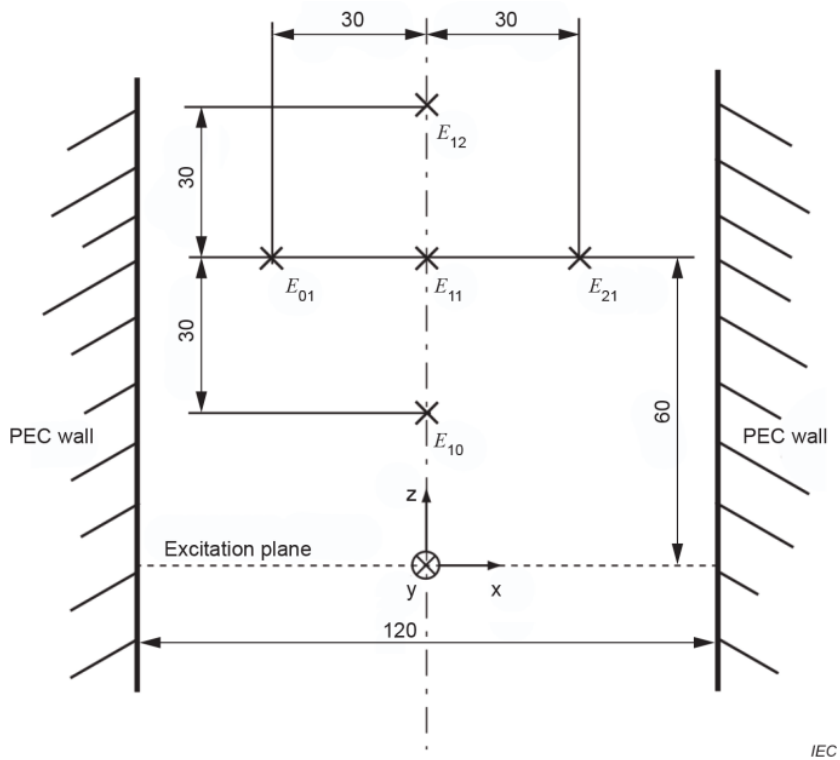


Figure 10 Aligned rectangular waveguide and locations of the sample points E01, E10, E11, E12 and E21 at which the Ex-components are recorded

Quantity	Limit	TE-pol			TM-pol		
ϵ_r		1	2	2	1	2	2
σ		0	0	0.2	0	0	0.2
max. dev. of simulated Re {Kz } from numerical reference 5 % above cut-off	$\pm 2\%$	0%	0.12%	-0.06%	0.01%	0.04%	1.02%
max. dev. of simulated Im {Kz } from numerical reference 5 % above cut-off	$\pm 2\%$	0.0038%	0.22%	-0.23%	0.89%	1.21%	0.765%
max. dev. of simulated Re {Kz from numerical reference 5 % above cut-off	$\pm 2\%$	/	/	0.12%	/	/	0.96%
max. dev. of simulated Im {Kz} from numerical reference 5 % above cut-off	$\pm 2\%$	/	/	0.0321%	/	/	-1.09%

Table 9 Results of the evaluation of the numerical dispersion characteristics to be reported for each mesh axis and each orientation of the waveguide for at least three increasing numbers of DoF

A.1.2 Planar dielectric boundaries

The implementation of planar dielectric interfaces shall be tested using the waveguide configurations described in A.1.1 (waveguide, excitation, frequencies) as a function of the number of DoF. The dielectric interface shall be perpendicular to the z-axis. A dielectric boundary shall be introduced at a

distance of 120 mm or larger from the excitation. The dielectric boundary is oriented perpendicularly to the PEC walls and divides the waveguide into two regions. A permittivity $\epsilon_r = \epsilon_1 = 1$ shall be used for the region that contains the excitation. The permittivity of the other region shall be $\epsilon_r = \epsilon_2 = 4$. A lossless (TE- and TM-polarization) and a lossy dielectric (TE-polarization only) shall be simulated ($\sigma = 0$ and $\sigma = 0.2$ S/m). The dielectric region extends to the end of the computational domain, and the length of the waveguide shall be chosen such that reflections from the mesh truncation of the computational domain do not reach the location at which the fields are recorded during the simulation

The numerical reflection coefficient as a function of the frequency shall be extracted from the complex electric field strength amplitudes at the positions in Figure 9 (see A.1.1). Closed-form expressions for the reflection coefficients for TE- and TM-polarization are in accordance with Equation (9) through Equation (12).

$$\rho_{TE} = \frac{k_{2z}}{k_{1z}} \quad (9)$$

$$r_{TE} = \frac{1 - \rho_{TE}}{1 + \rho_{TE}} \quad (10)$$

$$\rho_{TM} = \frac{\epsilon_1 k_{2z}}{\epsilon_2 k_{1z}} \quad (11)$$

$$r_{TM} = \frac{1 - \rho_{TM}}{1 + \rho_{TM}} \quad (12)$$

k_{1z} and k_{2z} are the wave numbers in the two dielectrics according to Equation (8) (see A.1.1). $\epsilon_1 = \epsilon_2$ and are required for the evaluation of $r_{TE} = r_{TM}$.

For the evaluation of the numerical reflection coefficient, the steps for the extraction of the numerical wave number in free space as described in A.1.1 shall be repeated. The numerical reflection coefficient shall then be evaluated in accordance with the following steps:

a) Extraction of the reflection coefficient – The amplitudes of the propagating and the reflected waves E_p and E_r are given by Equation (13) through Equation (14).

$$E_p = \frac{1}{\Psi} \left[E_{10} e^{-jk_z(2z_r - z_0 - z_{11})} - E_{11} e^{-jk_z(2z_r - z_0 - z_{10})} \right] \quad (13)$$

$$E_r = \frac{1}{\Psi} \left[E_{11} e^{-jk_z(z_{10} - z_0)} - E_{10} e^{-jk_z(z_{11} - z_0)} \right] \quad (14)$$

Where

$$\Psi = e^{-jk_z[2(z_r - z_0) + z_{10} - z_{11}]} - e^{-jk_z[2(z_r - z_0) + z_{11} - z_{10}]} \quad (15)$$

Here, z_r , and z_0 are the locations of the boundary and the source. z_{10} and z_{11} are the positions of the electric field sample points as shown in Figure 9 (see A.1.1). k_x , k_{1z} , and k_{2z} are the components of the numerical wave vector evaluated using Equation (3) and Equation (4) (see A.1.1). The amplitude reflection coefficient r is then calculated in accordance with Equation (16).

$$r = \frac{E_r}{E_p} \quad (16)$$

For the evaluation of k_{2z} the arrangement of the sample points shown in Figure 9 shall be repeated in the region filled with the dielectric ϵ_2 .

b) Data reporting – The numerical reflection coefficient r shall be evaluated as a function of the frequency for reactive modes in a frequency range from 0,5

GHz to 0.6 GHz (below the cut-off frequency of the waveguides) and for propagating modes in a frequency range from 1.4 GHz to 2 GHz. Frequency steps of 25 MHz shall be applied. These deviations shall be following the tolerance given in Table 5. In addition, the number of DoF at which the tolerance is reached shall be reported for each simulation. For the demonstration of convergence, the result shall be compared to the result of a coarser mesh with one-tenth the number of the DoF of the mesh of the final result. The deviation of the result of the coarser mesh from the physical result shall be larger than the deviation of the result from the physical result.

Quantity	Limit	TE-pol		TM-pol
ϵ_r		4	4	4
σ		0	0.2	0
max. dev. of simulated $\text{Re}\{k_{2z}\}$ from numerical reference 1.4 GHz < f < 2 GHz	$\pm 5\%$	0.39%	-0.28%	-0.37%
max. dev. of simulated $\text{Im}\{k_{2z}\}$ from numerical reference 0.5 GHz < f < 0.6 GHz	$\pm 5\%$	/	0.85%	/
max. dev. of simulated $\text{Re}\{r\}$ from numerical reference 1.4 GHz < f < 2 GHz	$\pm 5\%$	-0.45%	-0.93%	2.38%
max. dev. of simulated $\text{Im}\{r\}$ from numerical reference 1.4 GHz < f < 2 GHz	$\pm 5\%$	/	1.24%	/
max. dev. of simulated $\text{Re}\{r\}$ from numerical reference 0.5 GHz < f < 0.6 GHz	$\pm 10\%$	2.72%	2.45%	3.81%
max. dev. of simulated $\text{Im}\{r\}$ from numerical reference 0.5 GHz < f < 0.6 GHz	$\pm 10\%$	/	3.64%	/

Table 10 Results of the evaluation of the numerical reflection coefficient to be reported; frequency range is indicated for each value to be reported

A.2 Generic dipole

The following parameter were used in the dipole antenna to resonate at 148KHz to validate the accuracy of the tool at low frequencies.

Electromagnetic wavelength: 2027 meters

Dipole length: 1013.5 meters

Feed spacing: 6.757 meters

Dipole diameter: 13.514 meters

The quantities given in Table 11 shall be evaluated and compared to the indicated tolerance. The table 11 was demonstrated as shown below to show the validity of the model.

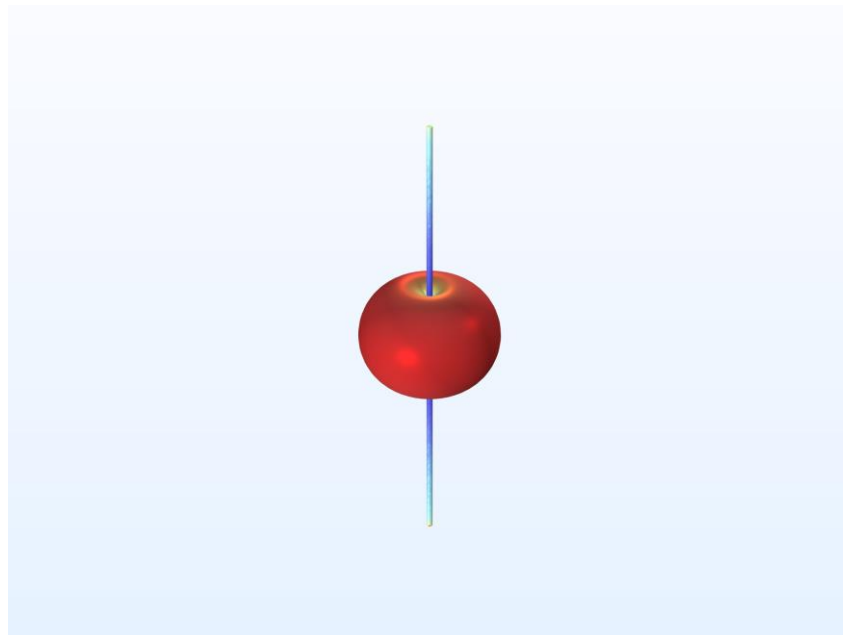


Figure 11 Dipole Antenna Model

Quantity	Simulation result	Tolerance	Satisfied?
Re(Z) at 148KHz	100.77	/	
Im(Z) at 148KHz	54.31	/	
Re(Z) at 118.4KHz	43.62	$25\Omega < Re(Z) < 50\Omega$	Yes
Im(Z) at 118.4KHz	-87.95	$-50\Omega < Im(Z) < -100\Omega$	Yes
Re(Z) at 133.2KHz	66.00	$50\Omega < Re(Z) < 75\Omega$	Yes
Im(Z) at 133.2KHz	-17.00	$-25\Omega < Im(Z) < 0\Omega$	Yes
Frequency for Im(Z)=0	136.6	$133.2KHz < f < 140.6KHz$	Yes
Maximum power budget error	0.37	< 5%	Yes

Table 11 Simulated Dipole parameters

A.3 Total Computational Uncertainty

Below is a table summarizing the budget of the uncertainty contributions of the numerical algorithm and of the rendering of the simulation setup.

Uncertainty Component	Probability distribution	Divisor f(d,h)	Uncertainty %
Mesh convergence	N	1	0.13%
Open boundary condition	N	1	0.21%
Power Budget	N	1	0.05%
Convergence of psSAR sampling	R	1.73	0.10%
Phantom dielectrics	R	1.73	0.00%
Combined std. uncertainty (k = 1)			0.48%

Table 12 Budget of uncertainty contributions of the numerical algorithm